

Constraint Maximal Inter-molecular Helix Lengths within RNA-RNA Interaction Prediction Improves Bacterial sRNA Target Prediction

Rick Gelhausen¹, Sebastian Will², Ivo L. Hofacker², Rolf Backofen^{1,3} and Martin Raden¹

¹Bioinformatics Group, University of Freiburg, Georges-Koehler-Allee 106, 79110 Freiburg, Germany

²Institute for Theoretical Chemistry, University of Vienna, Waehringer Strasse 17, 1090 Wien, Austria

³Centre for Biological Signalling Studies (BIOSS), University of Freiburg, Schaenzlestr. 18, 79104 Freiburg, Germany

Keywords: RNA-RNA Interaction Prediction, Steric Constraints, Constrained Helix Length, Canonical Helix, Seed.

Abstract: Efficient computational tools for the identification of putative target RNAs regulated by prokaryotic sRNAs rely on thermodynamic models of RNA secondary structures. While they typically predict RNA–RNA interaction complexes accurately, they yield many highly-ranked false positives in target screens. One obvious source of this low specificity appears to be the disability of current secondary-structure-based models to reflect steric constraints, which nevertheless govern the kinetic formation of RNA–RNA interactions. For example, often—even thermodynamically favorable—extensions of short initial kissing hairpin interactions are kinetically prohibited, since this would require unwinding of intra-molecular helices as well as sterically impossible bending of the interaction helix. In consequence, the efficient prediction methods, which do not consider such effects, predict over-long helices. To increase the prediction accuracy, we devise a dynamic programming algorithm that length-restricts the runs of consecutive inter-molecular base pairs (perfect canonical stackings), which we hypothesize to implicitly model the steric and kinetic effects. The novel method is implemented by extending the state-of-the-art tool INTARNA. Our comprehensive bacterial sRNA target prediction benchmark demonstrates significant improvements of the prediction accuracy and enables 3-4 times faster computations. These results indicate—supporting our hypothesis—that length-limitations on inter-molecular subhelices increase the accuracy of interaction prediction models compared to the current state-of-the-art approach.

1 INTRODUCTION

Small RNAs (sRNAs) are central regulators in prokaryotic cells (Storz et al., 2011). For instance, they can trigger mRNA decay (Lalaouna et al., 2013) or modulate translation (Hoe et al., 2013) via direct inter-molecular base pairing. Different mechanisms are known (detailed e.g. in (Nitzan et al., 2017)) like the blocking of the ribosomal binding site causing translation inhibition or the (de-)stabilization of mRNAs by covering (or providing) binding sites of RNAases. The sRNA–RNA interactions typically contain a small nearly perfect subinteraction of about 7 base pairs (known as *seed region*) (Künne et al., 2014) and have been shown to be located at accessible regions that are mainly unpaired (Richter and Backofen, 2012). Thus, beside general RNA–RNA interaction prediction approaches (reviewed e.g. in (Wright et al., 2018)), dedicated prediction tools like INTARNA (Busch et al., 2008) or RNAPREDATOR (Eggenhofer et al., 2011) have been developed and

applied (Li et al., 2012). Recently, fast heuristics for genome-wide screens have been implemented, e.g. RIBLAST (Fukunaga and Hamada, 2017) and RISEARCH2 (Alkan et al., 2017).

For elucidating the regulatory network of sRNAs, target prediction is applied (Backofen et al., 2014) to guide experimental validation. While the essential bioinformatics machinery for this task is available (Backofen et al., 2017), computational methods still predict a high number of false positive targets. The latter can be reduced when individual target predictions of homologous sequences (Lott et al., 2018) are combined in comparative approaches like COPRANA (Wright et al., 2014). Unfortunately, this technique is only applicable for the identification of evolutionary conserved targets. Another option is to incorporate experimental structure probing data to emend the RNAs' accessibility information (Miladi et al., 2019). Integrating probing data, which can be obtained from high-throughput experiments (Choudhary et al., 2017), can significantly alleviate the prob-

lem of inaccurate accessibility prediction. However, it does not touch—and is even orthogonal to—the here discussed issues of target prediction.

In this work, we study means to efficiently improve sRNA target prediction by restricting the admissible interaction patterns. This is hypothesized to incorporate steric and kinetic aspects going beyond the thermodynamic secondary structure-based models. Specifically, our method is motivated by the observation that interacting sites of sRNAs are either not enclosed by any base pairing (exterior) or located within loop regions. For loop regions, the formation of (long) inter-molecular helices (i.e. the entangling of the RNA molecules) requires the ‘unwinding’ of intra-molecular helices, which imposes additional constraints on the substantial steric rearrangements (rotating large parts of the molecules through space) while the interaction grows. Consequently, the formation of long inter-molecular duplexes seems to be prohibited, even if it would be expected in the currently used thermodynamic models due to high hybridization stability and sufficient accessibility. This well-known phenomenon has been studied in the context of other loop-initiated RNA–RNA interactions (Kolb et al., 2000; Brunel et al., 2002).

Concretely, we test whether interaction prediction can be improved by explicitly constraining the maximal length of inter-molecular helices, which—as we conjecture—indirectly considers steric and kinetic constraints. While preserving tractability, limiting this length ensures that long helices must be interrupted by interior loops—which is thought to relax the ‘winding tension’. We provide efficient dynamic programming algorithms both for exact as well as heuristic interaction prediction, incorporating the new helix-length constraint (in addition to the well-established seed constraint of previous approaches). The approach is incorporated into INTARNA (Mann et al., 2017), a state-of-the-art RNA–RNA interaction prediction tool (Umu and Gardner, 2017). Finally, we assess the effect of the helix-length constraints on a large prokaryotic sRNA target prediction data set extending (Wright et al., 2013). In this benchmark, the helix length limitation reduces the overall runtime and, supporting our conjecture, improves the prediction quality.

2 METHODS

In the following, we will first present the recursions used by the current state-of-the-art prediction approaches like RNAUP (Mückstein et al., 2006) or INTARNA (Mann et al., 2017). Subsequently, we in-

roduce the new recursions for helix-length restricted prediction. First, all recursions are given for exhaustive/optimal interaction prediction, followed with a discussion how they can be turned into efficient heuristic variants. To ease readability, we provide graphical recursion depictions and provide respective formulas in the Appendix.

2.1 Accessibility-based Interaction Prediction

Given two RNAs S_1, S_2 of length n, m , resp., we want to find the interaction sites $i..k \in [1, n]$ of S_1 and $j..l \in [1, m]$ of S_2 that minimize the interaction energy $E(i, j, k, l)$. That is, we are interested in the most stable interaction of an sRNA with a given putative target. This interaction energy can then be used for target ranking and the selection of the most promising candidates.

The interaction sites are considered free of intra-molecular base pairs and can only form inter-molecular base pairs. Two positions of the RNAs can form a base pair if the respective nucleotides are complementary (i.e. AU, GC, or GU). We consider only sites where the boundaries are forming two inter-molecular base pairs $(i, j), (k, l)$. No two inter-molecular base pairs $(x, y), (x', y') \in [1, n] \times [1, m]$ are allowed to be crossing, i.e. it holds $x \leq x' \leftrightarrow y \leq y'$, nor allowed to share a position within the same RNA. Following the Nearest Neighbor energy model (Tinoco Jr et al., 1973), the hybridization or duplex formation energy of a site is thus given by the sum of the loop energies (Turner and Mathews, 2010) defined by consecutive base pairs. Here, we distinguish between directly neighbored base pairs, scored by E_S terms, and neighbored base pairs that enclose unpaired positions, evaluated by E_{IL} terms. The hybridization energy also contains a general energy penalty term E_{init} that, to some extent, reflects the probability of interaction initiation. The optimal (minimal) hybridization energy among all possible interactions of the sites is given by $H(i, j, k, l)$. The energy penalty ED needed to break all intra-molecular base pairs within the individual sites is used to incorporate the sites’ accessibility for interaction formation. The overall energy of a site is thus given by

$$E(i, j, k, l) = H(i, j, k, l) + ED(i..k) + ED(j..l). \quad (1)$$

All energy terms presented in the following are given in $kcal/mol$ unit and are computed using the Vienna RNA package (Lorenz et al., 2011) version 2.4.4. For simplicity, we exclude dangling-end and helix-end contributions within Eq. 1. For formalisms, we refer to the detailed introduction provided in (Raden et al., 2018).

$$H_{j,l}^{i,k} = \min \begin{cases} E_{init}^{i,j,k} \\ E_S^{i,j+1,k} H_{j+1,l}^{i+1,k} \\ \min_{p,q} E_{IL}^{i,p,q,r} H_{q,l}^{p,r,k} \end{cases}$$

Figure 1: Sketch of the state-of-the-art recursion to compute the optimal interaction energy without further constraints.

$$helix_{j,l}^{i,k} = \min \begin{cases} E_S^{i,j+1,k} helix_{j+1,l}^{i+1,k} \\ E_S^{i,j,k} \end{cases}$$

$$H_{j,l}^{i,k} = \min \begin{cases} helix_{j,l}^{i,k} + E_{init} \\ \min_{p,q,r,s} helix_{q,l}^{p,r,k} E_{IL}^{i,p,q,r} H_{s,l}^{q,r,k} \end{cases}$$

Figure 2: Recursion depictions to compute canonical helix energies $helix$ (top) using energy terms E_S for stacked base pairs and the optimal energy H (bottom) for a given interaction site using the energy terms E_{IL} for interior loops.

ED terms can be efficiently computed via dynamic programming (Bernhart et al., 2011). This leaves the computation of the optimal interaction energy H , also accessible via dynamic programming (Mückstein et al., 2006). Figure 1 visualizes the central recursion that either scores an initial base pair (E_{init}) or extends a shorter optimal interaction with a stacked base pair (E_S) or an interior loop contribution (E_{IL}). All individual energy contributions E_{init} , E_S and E_{IL} are $+\infty$ if the respective boundary indices are non-complementary, i.e. can not form a base pair. Note, interior loop sizes ($p-r$ and $q-s$) are typically restricted to a fixed maximal length $w \ll n, m$, which results in a runtime complexity of $O(n^2m^2)$. A heuristic variant of this recursion available in INTARNA with $O(nm)$ runtime was introduced in (Busch et al., 2008). The base pairs of an optimal interaction with energy $H(i, j, k, l)$ can be obtained via traceback if of interest.

2.2 Helix-length Restricted Prediction

In order to restrict the length of inter-molecular helices to a predefined constant $c_B \geq 2$, referred to as *helix length*, we decompose the prediction process into two steps: (a) the energy pre-computation of possible helices composed of at most c_B base pairs, and (b) their assembly in order to find the optimal interaction energy for a given site.

For simplicity, we first consider canonical helices, i.e. perfect helices composed of stacked base pairs only. Adaptions to non-canonical helices con-

taining small bulges and interior loops are discussed in a subsequent section. Figure 2 shows the recursion to compute the energy of canonical helices with the left-/right-most inter-molecular base pair $(i, j) < (k, l)$, resp., stored in $helix(i, j, k, l)$. The length constraint c_B is ensured for canonical helices by setting all entries to $+\infty$ if the helix is too long, i.e. $\max(k - i, l - j) \geq c_B$. Note, for non-canonical helices, $helix(i, j, k, l)$ will contain the optimal energy of any helix fulfilling the relaxed constraints.

Given this, the optimal hybridization energy $H(i, j, k, l)$ for the given interaction sites $i..k$ and $j..l$ can be computed via the recursion depicted in Fig. 2. That is, we either consider a full helix (if possible for the given boundaries) or compose an interaction via the addition of a new helix (on the left) to extend a smaller optimal interaction. The composition inserts an interior loop between the helix and the next interaction to ensure that no two helices are combined into a longer one. Thus, the interior loop has to span at least one unpaired position, i.e. $(p - r) + (q - s) > 2$, and is constrained in length as for the recursions discussed before. Since both helix length as well as interior loop length are constrained by respective constants c_B and w , the overall runtime complexity is still $O(n^2m^2)$.

2.3 Enforcing Seed Constraints in Helix-length Restricted Prediction

As already discussed, seed-constraints are a central tool to reduce false positive sRNA target predictions (Tjaden et al., 2006; Bouvier et al., 2008). Within INTARNA, possible seed interactions and respective energies are efficiently computed via dynamic programming analogously to the presented helix energy pre-processing; please refer to (Busch et al., 2008) for details. In the following, the optimal energy for the seed with left-/right-most base pairs $(i, j), (k, l)$, resp., are stored in $seed(i, j, k, l)$.

In order to ensure that a reported interaction contains a seed region, we follow the approach presented in (Busch et al., 2008). Therein, a second dynamic programming table H_S is computed based on H that provides the optimal energy for a site given that the considered interaction contains a seed region. The optimal energy of a site with seed is then given by

$$E(i, j, k, l) = H_S(i, j, k, l) + ED(i..k) + ED(j..l) \quad (2)$$

replacing Eq. 1.

Since seeds are valid parts of helices, which are the building blocks for our introduced H computation, we use a second auxiliary matrix $helix_S$ that provides the optimal helix energy given that the helix contains

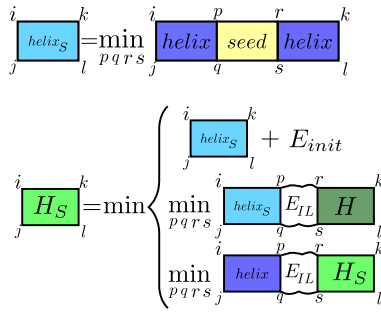


Figure 3: Depiction of the decomposition strategy for the computation of the optimal energy of a helix containing a seed $helix_S$ (top) and the best hybridization energy H_S (bottom) enforcing both the helix and seed constraint.

a seed. If the region contains no valid seed or this would lead to too many base pairs, the energy is set to $+\infty$. Figure 3 depicts the recursion in order to fill $helix_S$ based on the already introduced $helix$ information that is combined with the *seed* energy. To this end, all possible locations of a seed combined with flanking helices are evaluated. Due to the independence of the seed and helix constraints, it is possible to allow unpaired bases in the seed, even when not allowing unpaired bases in the helix constraints and vice versa.

Given this, the optimal hybridization energy H_S for a given site containing a seed and only helices with at most c_B base pairs, can be computed using a recursion as depicted in Fig. 3. That is, either (i) the site can be filled with a single helix containing a seed (plus accounting for interaction initiation), or (ii) a helix-length-constrained interaction site is extended with a seed-containing helix, or (iii) we extend an interaction that contains already a seed with a helix that is not constrained to contain a seed.

2.4 Enforcing a Minimal Helix Stability

Given our focus on helices, we can easily enforce additional constraints on the helices that are considered for interaction composition. As the first step, we introduce a minimal stability notion via an upper hybridization energy bound E_{max}^{helix} for individual helices. Since energy is inversely related to stability, our approach will produce interaction patterns of stable sub-helices connected by interior loop regions.

The energy threshold can be easily incorporated into the presented recursions by extending the computation of H and H_S from Fig. 2 and 3, resp., with side conditions. That is, entries from $helix$ or $helix_S$ are only considered, if the respective energy value is below the given threshold E_{max}^{helix} .

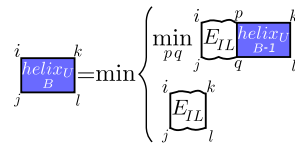


Figure 4: Recursion depiction to compute the optimal hybridization energy $helix_U(i, j, k, l, B)$ for non-canonical helices with exactly B base pairs and interior loops containing at most c_U unpaired bases, i.e. $(p - i) + (q - j) \leq c_U + 2$ and analogously for the second case.

2.5 Consideration of Non-canonical Helices

So far, we only considered canonical helices for the computation of $helix$. While this models the most stable helices that can be formed, minor variance of this ideal, i.e. allowing for bulges or interior loops spanning only single or very few unpaired bases, will still resemble a stable helix. But considering stable helices only (using E_{max}^{helix}) would likely exclude such helices if the canonical subhelices are too short. Thus, we next discuss how the hybridization energy $helix$ for helices including minor bulges of at most c_U unpaired bases can be computed. We consider an interior loop as minor if $c_U \leq 2$.

To this end, we introduce the auxiliary matrix $helix_U(i, j, k, l, B)$ that provides the optimal helix hybridization energy for the given site boundaries and the number of base pairs B while allowing minor bulges of size c_U . Figure 4 depicts the respective recursion. Note, the boundaries p, q considered for interior loops are constrained to $(p - i) + (q - j) \leq c_U + 2$. The optimal helix hybridization energy $helix(i, j, k, l)$ is thus given by $helix_U(i, j, k, l, c_B)$. Note, enforcing the helices to be stable (via E_{max}^{helix}) will without further constraints exclude helices composed of bulges only.

In addition to the altered $helix$ computation, we also have to ensure that the helices assembled within the H and H_S computation are spaced by interior loops exceeding c_U . That is, it holds for Fig. 2 and 3 that $(r - p) + (s - q) > c_U + 2$. Note that setting $c_U = 0$ will provide the same results as if using canonical helices only.

2.6 Heuristic Helix-length Restricted Prediction

Due to the high time and space complexity of the exact approach, we implemented heuristic variants of the recursions following the ideas from (Busch et al., 2008) introduced for INTARNA. That is, instead of considering all interaction ranges for a given left-most base pair (i, j) , only the optimal right boundary (k, l)

together with the respective hybridization energy is stored in H and H_S . Thus, for a given left-most base pair (i, j) , the recursions from above are not confined to a specific right k, l bound but use the right end of the respective optimal recursion case. Please refer to (Busch et al., 2008) for further details. This heuristic reduces the space and time complexity to $O(nm)$, provides almost the same prediction quality (Umu and Gardner, 2017), and makes the approach feasible for the needed large-scale target screens also discussed in the Result section.

Here, we apply this strategy not only to H and H_S but also to the *helix* and *helix_S* matrices. That is, we only memorize the best helix energy (and right boundary) for each left-most helix base pair (i, j) . Note, both matrices have to be computed using small auxiliary matrices that replace the respective recursions. Note further, the computation of H and H_S becomes more simple, since we do not consider different helix lengths (via p and q) but only use the right-most base pair of the best helix with left-most base pair (i, j) .

3 RESULTS

To evaluate our introduced predictors concerning their sRNA target prediction performance, we introduce the manually curated benchmark data used subsequently.

3.1 Data Set for sRNA Target Prediction Benchmark

We investigate whether a restriction on inter-molecular helix lengths could improve the overall prediction accuracy of INTARNA. To this end, we created an sRNA target prediction benchmark extending the ideas and data from (Wright et al., 2013). The whole benchmark data set including respective scripts is available at:

<https://github.com/BackofenLab/IntaRNA-benchmark>.

The benchmark consists of a large set of bacterial sRNA queries and potential target sequences. We restrict our analysis to sRNA regulation based on the blocking of the ribosomal binding site (see (Nitzan et al., 2017) for a discussion). Thus, the targets are genomic sub-regions around the start codon of the respective mRNA including 200 nucleotides upstream and 100 nucleotides downstream, since many sRNAs that regulate translation bind their target in a region around the start codon. Sequences are extracted from the GenBank database of the National

Centre for Biotechnology Information (NCBI) (Benson et al., 2008). The dataset comprises 4,319 target regions from the *E.coli* genome (GenBank accession number NC_000913) and 4,552 target regions from the *Salmonella typhimurium* genome (NC_003197). The query data set consists of 15 sRNAs from *E. coli* and 15 from *Salmonella*, which have been shown experimentally to act as post-transcriptional regulators by base-pairing to at least one of the target mRNAs.

To evaluate the performance, we follow the approach from (Tjaden et al., 2006). To this end, we extracted 149 sRNA-mRNA pairs from the literature that have been experimentally verified to interact. Within the benchmark, we test how well these verified pairs can be separated from all possible sRNA-mRNAs pairs. That is, we predict the optimal interaction energy E for each of the 15 sRNAs in *E.coli* with any of the 4,319 putative target regions. The same is done for the *Salmonella* data set. As a result, there are in total 133,065 potential sRNA-target interactions and respective interaction energy estimates. From these, only the mentioned 149 query-target pairs are supported, leaving 132,916 unsupported pairs. Finally, we test whether interactions of the verified pairs have lower optimal energy estimates compared to the unsupported interactions. In other words, we evaluate the ranks of the supported pairs within the energy score distribution over all putative targets. That is, the more verified interactions are predicted with low rank, the more precise is the target prediction approach. A detailed description of the technical part is available in the Appendix.

3.2 Helix-length Constraints Enable Faster Predictions and Improve Prediction Quality

As reference and "gold standard" for the evaluation of our helix-length restricted approach, we use the prediction performance of INTARNA version 2.2.0 using default values (i.e. heuristic predictions including seeds) on the introduced benchmark data set using a seed of length 7 for all predictions. In the following, we refer to this version with "original".

Effect of Maximal Helix Length

We have extended INTARNA with implementations of our heuristic recursions, which enables clean comparisons for both prediction quality as well as space and runtime requirement of the computations. Figure 5 compares the results for different maximal helix length values c_B with the original predictions. The

Performance for length-limited canonical stacks containing a seed

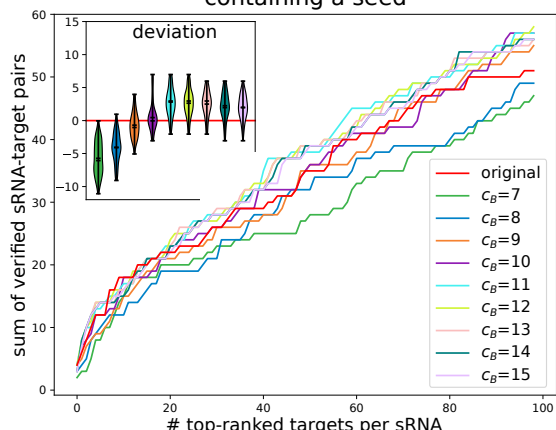


Figure 5: Effect of different maximal canonical helix lengths c_B in terms of the recovery of verified sRNA-target pairs among the top ranked predictions compared to the original INTARNA results (red curve). The inset shows the differences to the original results (red).

curves visualize the total number of verified sRNA-target pairs within the respective top-ranked predictions for each sRNA. That is the higher the curve the better the recovery rate of the verified targets. To ease comparisons, the inset shows the difference between the results of the *original* version (red curve) and the respective helix-length constrained predictions.

For low c_B values, we observe a reduced prediction accuracy compared to the original recursions. In contrast, maximal helix lengths of 11-13 show much improved recovery rates and provide the overall best results. For $c_B = 11$, we observe the highest recovery improvement of additional 2.7 verified targets on average. Higher c_B values have a lower prediction accuracy that will eventually converge towards the unconstrained original prediction results. These observations apply to all tested variants.

In addition to the higher prediction accuracy, the constrained version is about 3-4 times faster compared to the original version, while maintaining the same memory consumption.

Effect of Minimal Helix Stability

Next, we investigate whether the restriction to stable helices can further improve the prediction quality. To this end, we fixed the maximal helix length to $c_B = 11$, given the results from above, and tested different helix hybridization energy thresholds E_{max}^{helix} . Figure 6 summarizes the results. $E_{max}^{helix} = -7.5$ shows best performance with a recovery improvement of about 8 verified targets on average, which is about three-times higher compared to $c_B = 11$ results without sta-

Performance for stable length-limited canonical stacks containing a seed

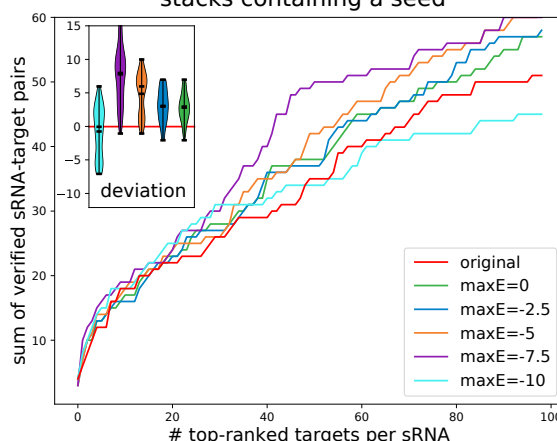


Figure 6: Effect of different maximal helix energies E_{max}^{helix} (maxE in the plot) on the prediction performance (maximal canonical helix length $c_B = 11$) analogously to Fig. 5.

Best performing parameterizations

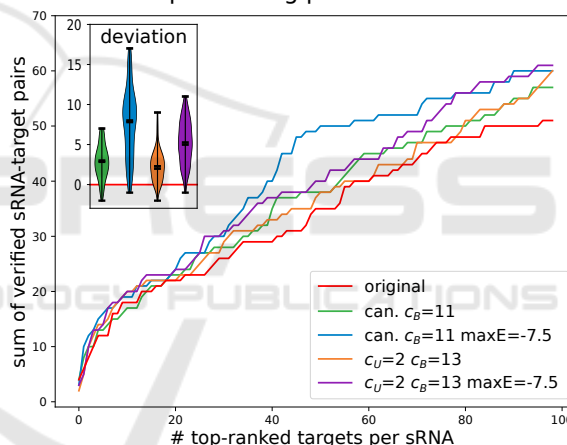


Figure 7: Overview of the best prediction performance for canonical (can.) (maximal canonical helix length $c_B = 11$) and non-canonical ($c_U = 2$) (maximal canonical helix length $c_B = 13$) and the overall best $E_{max}^{helix} = -7.5$ for both methods. Plot analogously to Fig. 5.

bility constraint (see above). Note, all tested E_{max}^{helix} values above -7.5 provide improved prediction performance. Too low thresholds ($E_{max}^{helix} = -10$) exclude too many helices to enable better target prediction.

Effect of Non-canonical Helices

When relaxing the helix definition to non-canonical helices that are allowed to contain minor bulges or interior loops with up to c_U unpaired bases, the overall prediction performance is not exceeding the canonical helix variant. Here, best results are observed for $c_U = 2$ and a maximal helix length $c_B = 13$ while c_B values

of 11-13 still show the best results (data not shown). Figure 7 provides a comparison of the best parameterizations for the canonical and non-canonical approach with and without $E_{\max}^{\text{helix}} = -7.5$ constraint. From this it is obvious that a relaxation of the helix definition does not improve the prediction quality compared to stable canonical helices.

4 DISCUSSION & CONCLUSION

Predictions of helix-length constrained interactions can be done with the same time and space complexity as known for unconstrained RNA-RNA interaction prediction. In fact, the helix-length constraint significantly reduces the search space such that we observe on average a 3-4 times faster target prediction for our benchmark data set. The reduced runtime results from the following: compared to the current state-of-the-art recursion from Fig. 1, the helix-length constrained approach from Fig. 2 faces the same search space for the interior loop sizes but appends full helices instead of individual base pairs. This becomes even more striking for the heuristic variant, which does not consider all possible helix lengths but only the optimal helix for the left-most base pair (i, j) .

Furthermore, we observe enriched target prediction accuracy measured in terms of increased recovery rates of verified sRNA-target pairs known from the literature. Maximal helix lengths c_B of 11-13 base pairs show the best prediction quality, while shorter drastically reduced the recovery rate. This is mainly achieved by disregarding low-energy interactions composed of many bulge and interior loops (putative false positives) rather than altering the interaction details of the verified sRNA-target pairs. Results can be further improved when only stable helices with an energy below a given threshold E_{\max}^{helix} are considered for prediction. For helices of a maximal length of 11-13 base pairs, an upper energy bound of -7.5 kcal/mol provides the best target prediction performance. Notably, the consideration of a relaxed helix definition allowing for small bulge or interior loops does not significantly improve the results compared to perfect canonical helices but has slightly higher runtime requirements.

Our observations support our hypothesis that long inter-molecular helices are less likely due to steric and kinetic constraint of the interaction formation process. That is, we think the 'decomposed helix interaction model', where short stable helices are interrupted by flexible interior loops, a more realistic model compared to unconstrained predictions.

One way to further improve the model would be

to confine helix-length constrained predictions to regions mainly unpaired in loop regions while applying the unconstrained approach for exterior unpaired regions. This can be efficiently distinguished during ED computation from the underlying partition functions (Mückstein et al., 2006; Bernhart et al., 2011). Another planned direction is to apply further constraints on the helices considered within the prediction. For instance, we will further investigate the correlation of helix base pair number c_B and optimal upper energy bounds E_{\max}^{helix} , since they are most likely linked by the average stacking energy or similar terms.

Even though we exemplified our new approach by extending INTARNA, the concept is a generic one. We therefore expect also other RNA-RNA interaction prediction methods to profit from a restriction of inter-molecular helix lengths.

ACKNOWLEDGEMENTS

This work was supported by the German Research Foundation (DFG) [BA2168/16-1] and the Austrian Science Fund (FWF) [I 2874-N28].

REFERENCES

- Alkan, F., Wenzel, A., Palasca, O., Kerpedjiev, P., Rudebeck, A., Stadler, P. F., Hofacker, I. L., and Gorodkin, J. (2017). RIssearch2: suffix array-based large-scale prediction of RNARNA interactions and siRNA off-targets. *Nucleic Acids Research*, 45(8):e60.
- Backofen, R., Amman, F., Costa, F., Findeiss, S., Richter, A. S., and Stadler, P. F. (2014). Bioinformatics of prokaryotic RNAs. *RNA Biol*, 11(5).
- Backofen, R., Engelhardt, J., Erxleben, A., Fallmann, J., Grüning, B., Ohler, U., Rajewsky, N., and Stadler, P. F. (2017). RNA-bioinformatics: Tools, services and databases for the analysis of RNA-based regulation. *J Biotechnol*, 261:76–84.
- Benson, D. A., Karsch-Mizrachi, I., Lipman, D. J., Ostell, J., and Wheeler, D. L. (2008). GenBank. *Nucleic Acids Res.*, 36(Database issue):25–30.
- Bernhart, S. H., Mückstein, U., and Hofacker, I. L. (2011). RNA accessibility in cubic time. *Algorithms for Molecular Biology*, 6(1):3.
- Bouvier, M., Sharma, C. M., Mika, F., Nierhaus, K. H., and Vogel, J. (2008). Small RNA binding to 5' mRNA coding region inhibits translational initiation. *Mol. Cell*, 32(6):827–837.
- Brunel, C., Marquet, R., Romby, P., and Ehresmann, C. (2002). RNA loop-loop interactions as dynamic functional motifs. *Biochimie*, 84(9):925 – 944.
- Busch, A., Richter, A. S., and Backofen, R. (2008). IntaRNA: efficient prediction of bacterial sRNA targets incorporating target site accessibility and seed regions. *Bioinformatics*, 24(24):2849–56.

- Choudhary, K., Deng, F., and Aviran, S. (2017). Comparative and integrative analysis of RNA structural profiling data: current practices and emerging questions. *Quantitative Biology*, 5(1):3–24.
- Eggenhofer, F., Tafer, H., Stadler, P. F., and Hofacker, I. L. (2011). RNApredator: fast accessibility-based prediction of sRNA targets. *Nucleic Acids Res*, 39(Web Server issue):W149–54.
- Fukunaga, T. and Hamada, M. (2017). RIBlast: an ultrafast RNARNA interaction prediction system based on a seed-and-extension approach. *Bioinformatics*, 33(17):2666–2674.
- Hoe, C.-H., Raabe, C. A., Rozhdestvensky, T. S., and Tang, T.-H. (2013). Bacterial sRNAs: Regulation in stress. *International Journal of Medical Microbiology*, 303(5):217 – 229.
- Kolb, F. A., Malmgren, C., Westhof, E., Ehresmann, C., Ehresmann, B., Wagner, E. G., and Romby, P. (2000). An unusual structure formed by antisense-target RNA binding involves an extended kissing complex with a four-way junction and a side-by-side helical alignment. *RNA*, 6(3):311–324.
- Künne, T., Swarts, D. C., and Brouns, S. J. (2014). Planting the seed: target recognition of short guide RNAs. *Trends in Microbiology*, 22(2):74 – 83.
- Lalaouna, D., Simoneau-Roy, M., Lafontaine, D., and Mass, E. (2013). Regulatory RNAs and target mRNA decay in prokaryotes. *Biochimica et Biophysica Acta (BBA) - Gene Regulatory Mechanisms*, 1829(6):742 – 747. RNA Decay Mechanisms.
- Li, W., Ying, X., Lu, Q., and Chen, L. (2012). Predicting sRNAs and their targets in bacteria. *Genomics, Proteomics & Bioinformatics*, 10(5):276 – 284.
- Lorenz, R., Bernhart, S. H., Höner zu Siederdisen, C., Tafer, H., Flamm, C., Stadler, P. F., and Hofacker, I. L. (2011). ViennaRNA Package 2.0. *Algorithms for Molecular Biology*, 6(1):26.
- Lott, S. C., Schäfer, R. A., Mann, M., Backofen, R., Hess, W. R., Voss, B., and Georg, J. (2018). GLASSgo - automated and reliable detection of sRNA homologs from a single input sequences. *Frontiers in Genetics*, 9:124.
- Mann, M., Wright, P. R., and Backofen, R. (2017). IntaRNA 2.0: enhanced and customizable prediction of RNA-RNA interactions. *Nucleic Acids Res.*, 45(W1):W435–W439.
- Miladi, M., Montaseri, S., Backofen, R., and Raden, M. (2019). Integration of accessibility data from structure probing into RNA-RNA interaction prediction. *Bioinformatics*, (epub ahead of print).
- Mückstein, U., Tafer, H., Hacker Müller, J., Bernhart, S. H., Stadler, P. F., and Hofacker, I. L. (2006). Thermodynamics of RNA–RNA binding. *Bioinformatics*, 22(10):1177–1182.
- Nitzan, M., Rehani, R., and Margalit, H. (2017). Integration of bacterial small RNAs in regulatory networks. *Annual Review of Biophysics*, 46(1):131–148.
- Raden, M., Mohamed, M. M., Ali, S. M., and Backofen, R. (2018). Interactive implementations of thermodynamics-based RNA structure and RNA-RNA interaction prediction approaches for example-driven teaching. *PLOS Comput. Biol*, 14(8):e1006341.
- Richter, A. S. and Backofen, R. (2012). Accessibility and conservation: General features of bacterial small RNA-mRNA interactions? *RNA Biol*, 9(7):954–65.
- Storz, G., Vogel, J., and Wassarman, K. (2011). Regulation by small RNAs in bacteria: Expanding frontiers. *Molecular Cell*, 43(6):880 – 891.
- Tinoco Jr, I., Borer, P., Dengler, B., Levin, M., Uhlenbeck, O., Crothers, D., and Bralla, J. (1973). Improved estimation of secondary structure in ribonucleic acids. *Nature New Biology*, 246(150):40–41.
- Tjaden, B., Goodwin, S. S., Opdyke, J. A., Guillier, M., Fu, D. X., Gottesman, S., and Storz, G. (2006). Target prediction for small, noncoding RNAs in bacteria. *Nucleic Acids Res.*, 34(9):2791–2802.
- Turner, D. H. and Mathews, D. H. (2010). NNDB: the nearest neighbor parameter database for predicting stability of nucleic acid secondary structure. *Nucleic Acids Res*, 38(Database issue):D280–2.
- Umu, S. U. and Gardner, P. P. (2017). A comprehensive benchmark of RNA-RNA interaction prediction tools for all domains of life. *Bioinformatics*, 33(7):988–996.
- Wright, P. R., Georg, J., Mann, M., Sorescu, D. A., Richter, A. S., Lott, S., Kleinkauf, R., Hess, W. R., and Backofen, R. (2014). CopraRNA and IntaRNA: predicting small RNA targets, networks and interaction domains. *Nucleic Acids Res.*, 42(Web Server issue):W119–23.
- Wright, P. R., Mann, M., and Backofen, R. (2018). Structure and interaction prediction in prokaryotic RNA biology. *Microbiol Spectrum*, 6(2).
- Wright, P. R., Richter, A. S., Papenfort, K., Mann, M., Vogel, J., Hess, W. R., Backofen, R., and Georg, J. (2013). Comparative genomics boosts target prediction for bacterial small RNAs. *Proceedings of the National Academy of Sciences*, 110(37):E3487–96.

APPENDIX

A Benchmarking Workflow

The benchmark workflow used for the creation of the prediction accuracy plots is shown in Figure 8. First, for each sRNA query, optimal interactions with all mRNA targets are predicted using INTARNA with a certain parameter set. Then the resulting interactions are sorted according to their energy values, from the most favourable, i.e. those with the lowest values, to the least favourable. Finally, we identify the rank of each verified target (considered a supported prediction). For each maximal rank value (later plotted on the x-axis), we count the number of verified targets for all sRNA queries that show a rank smaller or equal to this.

This process is repeated for each benchmarked parameter set. The data collected is then plotted. The

x-axis of the plot represents the maximal rank we consider for each result file, e.g. a number of target predictions of 20 means that we consider the 20 first lines of each result file and count how many verified targets appear. This is covered by the y-axis, which represents how many verified targets were among the considered top-ranked target predictions. The violin plots are generated by calculating the difference of a certain parameterization of INTARNA e.g. $c_B = 11$ to the original predictor. This reveals general trends of the different methods compared to the curve plot.

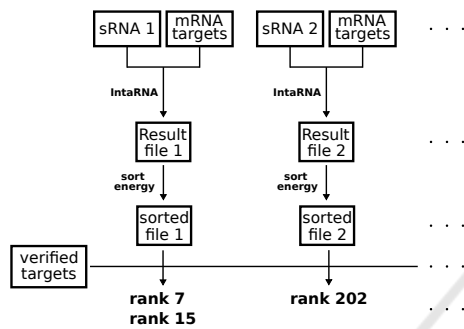


Figure 8: Depiction of the benchmarking process.



B Formal Recursions

$$E_S(i, j, k, l) = \begin{cases} \left(\begin{array}{l} \text{energy contribution for} \\ \text{stacking base pairs } (i, j), (k, l) \end{array} \right) & : \text{ if } k - i = 1 \text{ and } l - j = 1, \\ +\infty & : \text{ otherwise} \end{cases} \quad (3)$$

$$E_{IL}(i, j, k, l) = \begin{cases} \left(\begin{array}{l} \text{energy contribution for} \\ \text{stack or interior loop } (i, j), (k, l) \end{array} \right) & : \text{ if } i < k \text{ and } j < l, \\ +\infty & : \text{ otherwise} \end{cases} \quad (4)$$

$$helix(i, j, k, l) = \begin{cases} \min \begin{cases} E_S(i, j, i + 1, j + 1) + helix(i + 1, j + 1, k, l) \\ E_S(i, j, k, l) \end{cases} & : \text{ if canonical helix} \\ helix_U(i, j, k, l; c_U, c_B) & : \text{ otherwise} \end{cases} \quad (5)$$

$$helix_U(i, j, k, l; U, B) = \min \begin{cases} \min_{\substack{p, q \text{ with} \\ \min(k-p, l-q) \geq B-1 \\ (p-i)+(q-j) \leq U+2}} \left(\begin{array}{l} E_{IL}(i, j, p, q) \\ + helix_U(p, q, k, l; U, B-1) \end{array} \right) & : \text{ if } B > 2, \\ E_{IL}(i, j, k, l) & : \text{ otherwise.} \end{cases} \quad (6)$$

$$helix_S(i, j, k, l) = \min_{\substack{p, r \\ q, s}} (helix(i, j, p, q) + seed(p, q, r, s) + helix(r, s, k, l)) \quad (7)$$

$$H(i, j, k, l) = \min \begin{cases} helix(i, j, k, l) + E_{init} \\ \min_{\substack{p, r, q, s \text{ with} \\ (r-p)+(s-q) > c_U + 2 \\ helix(i, j, k, l) \leq E_{max}^{helix}}} \left(helix(i, j, p, q) + E_{IL}(p, q, r, s) + H(r, s, k, l) \right) \end{cases} \quad (8)$$

$$H_S(i, j, k, l) = \min \begin{cases} helix_S(i, j, k, l) + E_{init} \\ \min_{\substack{p, r, q, s \text{ with} \\ (r-p)+(s-q) > c_U + 2 \\ helix_U(i, j, k, l) \leq E_{max}^{helix}}} \left(helix_S(i, j, p, q) + E_{IL}(p, q, r, s) + H(r, s, k, l) \right) \\ \min_{\substack{p, r, q, s \text{ with} \\ (r-p)+(s-q) > c_U + 2 \\ helix(i, j, k, l) \leq E_{max}^{helix}}} \left(helix(i, j, p, q) + E_{IL}(p, q, r, s) + H_S(r, s, k, l) \right) \end{cases} \quad (9)$$